RAA 2016 Vol. **16** No. **5**, 77 (10pp) doi: 10.1088/1674–4527/16/5/077
http://www.raa-journal.org *http://iopscience.iop.org/raa*

***R**esearch in*
***A**stronomy and*
***A**strophysics*

Broad-band spectroscopy of the transient X-ray binary pulsar KS 1947+300 during 2013 giant outburst: Detection of pulsating soft X-ray excess component

Prahlad Epili, Sachindra Naik and Gaurava K. Jaisawal

Astronomy and Astrophysics Division, Physical Research Laboratory, Ahmedabad 380009, India; *prahlad@prl.res.in (PE); snaik@prl.res.in (SN); gaurava@prl.res.in (GKJ)*

Received 2015 August 19; accepted 2016 February 11

Abstract We present the results obtained from detailed timing and spectral studies of the Be/X-ray binary pulsar KS 1947+300 during its 2013 giant outburst. We used data from *Suzaku* observations of the pulsar at two epochs, i.e. on 2013 October 22 (close to the peak of the outburst) and 2013 November 22. X-ray pulsations at $\sim$18.81 s were clearly detected in the light curves obtained from both observations. Pulse periods estimated during the outburst showed that the pulsar was spinning up. The pulse profile was found to be single-peaked up to $\sim$10 keV beyond which a sharp peak followed by a dip-like feature appeared at hard X-rays. The dip-like feature has been observed up to $\sim$70 keV. The 1–110 keV broad-band spectroscopy of both observations revealed that the best-fit model was comprised of a partially absorbed Negative and Positive power law with EXponential cutoff (NPEX) continuum model along with a blackbody component for the soft X-ray excess and two Gaussian functions at 6.4 and 6.7 keV for emission lines. Both the lines were identified as emission from neutral and He-like iron atoms. To fit the spectra, we included the previously reported cyclotron absorption line at 12.2 keV. From the spin-up rate, the magnetic field of the pulsar was estimated to be $\sim 1.2\times10^{12}$ G and found to be comparable to that obtained from the detection of the cyclotron absorption feature. Pulse-phase resolved spectroscopy revealed the pulsating nature of the soft X-ray excess component in phase with the continuum flux. This confirms that the accretion column and/or accretion stream are the most probable regions of the soft X-ray excess emission in KS1947+300. The presence of the pulsating soft X-ray excess in phase with continuum emission may be the possible reason for not observing the dip at soft X-rays.

Key words: pulsars: individual (KS 1947+300) — stars: neutron — X-rays: binaries

1 INTRODUCTION

Be/X-ray binaries (BeXBs) are known to be the largest subclass ($\sim$60%) of high-mass X-ray binaries (Caballero & Wilms 2012). The majority of BeXBs consist of a neutron star as a compact object and a Be star as an optical companion. The optical companions in these binary systems are non-supergiant B-type stars of luminosity class III-V that show emission lines in their optical/infrared spectra (Okazaki & Negueruela 2001; Reig 2011). The neutron star in BeXBs accretes matter from the circumstellar disk of the Be star, usually at the periastron passage. This abrupt accretion of a huge amount of matter causes significant enhancement of the X-ray emission from the pulsating neutron star. These periodic enhancements of the X-ray intensity are known as Type I X-ray outbursts (peak luminosity $\sim 10^{35}-10^{37}$ erg s^{-1}). The neutron star in these systems, however, occasionally shows rare X-ray outbursts (Type II), lasting for several tens of days to a few months during which the peak luminosity reaches up to 10^{38} erg s^{-1}. For a brief review of the properties of BeXBs, refer to Paul & Naik (2011).

The transient BeXB pulsar KS 1947+300 was discovered on 1989 June 8 with the *Kvant/TTM* coded-mask X-ray spectrometer on the *Mir* space station (Skinner 1989; Borozdin et al. 1990). The pulsar was first detected at a flux level of 70 mCrab that later decreased to $\sim$10 mCrab within 2 months of the detection. The spectra obtained from these observations were described by an absorbed power-law with a photon index of 1.72$\pm$0.31 (Borozdin et al. 1990).

In April 1994, the X-ray pulsar GRO J1948+32 was discovered close to the coordinates of KS 1947+300 by the Burst and Transient Source Experiment (BATSE) instrument onboard the *Compton Gamma Ray Observatory (CGRO)* (Chakrabarty et al. 1995). The pulsation from this new source was found to be 18.7 s. Based on the spin period analysis, later Swank & Morgan (2000) established that KS 1947+300 and GRO J1948+32 are the same source. A Be star with a visible magnitude of 14.2 at a dis-

tance of ∼10 kpc was discovered as the optical counterpart of the pulsar (Negueruela et al. 2003).

KS 1947+300 was inactive from 1995 to 2000 without showing any major X-ray outburst. Subsequent *RXTE* observations showed that the source became active in October 2000 and went into a strong X-ray outburst (Levine & Corbet 2000). The pulsar spectrum in the 2–80 keV range during the outburst was described with a Comptonization continuum model along with a blackbody component for the soft X-ray excess and a Gaussian component for the iron emission line at 6.5 keV (Galloway et al. 2004). The orbital parameters of the binary system were also estimated from observations during October and are reported in Galloway et al. (2004). A glitch in the pulsar frequency, generally seen in anomalous X-ray pulsars and radio pulsars, but which is rare in accretion powered X-ray pulsars, was first detected in KS 1947+300 (Galloway et al. 2004). A low frequency quasi-periodic oscillation (QPO) at 20 mHz was detected on several occasions in the declining phase of the 2001 outburst with *RXTE* (James et al. 2010). Detection of low frequency QPOs and strong pulsations at low luminosity levels indirectly indicated that the magnetic field of the neutron star is $< 10^{13}$ G as predicated from spin-up torque and luminosity correlation (James et al. 2010). Using *BeppoSAX* observations of the 2001 X-ray outburst, Naik et al. (2006) described the broad-band pulsar spectrum in 0.1–100 keV with a Comptonization model along with a blackbody component at ∼0.6 keV and detected a weak 6.7 keV emission line from helium-like iron atoms. However, the iron Kα emission line was absent in the spectrum during the 2001 outburst.

A series of weak outbursts was observed from KS 1947+300 during the period of 2002–2004. Among these outbursts, the strongest one was detected with *INTEGRAL* in April 2004. A high energy cutoff power-law model was used to describe the spectra obtained from *INTEGRAL/ISGRI* and *JEM-X* data during this outburst (Tsygankov & Lutovinov 2005). However, there was no signature of cyclotron absorption lines in the pulsar spectra. In October 2013, KS 1947+300 was detected in a giant outburst with a peak flux of 130 mCrab in the 3–10 keV range (Fürst et al. 2014). Several *Swift/XRT* and three *NuSTAR* pointed observations were performed at different phases of the X-ray outburst. Combined spectra from *Swift/XRT* and *NuSTAR* in the 0.8–79 keV range were described by a power law with an exponential cutoff continuum model along with a blackbody and an iron line component at 6.5 keV (Fürst et al. 2014). A cyclotron absorption line at ∼12.2 keV was discovered in the pulsar spectra only during the second *NuSTAR* observation. The surface magnetic field of the pulsar was estimated to be $\sim 1.1 \times 10^{12}(1+z)$ G. Although KS 1947+300 had gone through several major X-ray outbursts, the cyclotron absorption line was not detected in the spectra obtained from earlier *RXTE*, *BeppoSAX* or *INTEGRAL* observations.

As the October 2013 outburst was a giant outburst, the pulsar was active for a few months during which it was observed with different X-ray observatories. We have used two *Suzaku* observations of the pulsar during this outburst to study its broad-band timing and spectral properties. The details on the observations, analysis, results and conclusions are presented in the following sections of the paper.

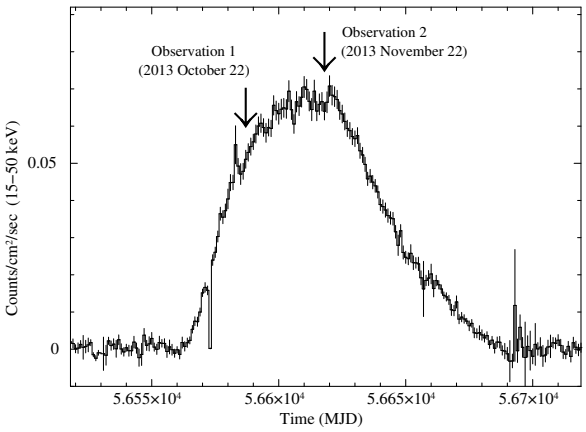

Fig. 1 *Swift/BAT* light curve of KS 1947+300 in the 15–50 keV energy range from 2013 August 14 (MJD 56518) to 2014 March 03 (MJD 56719). The arrow marks in the figure show the dates of *Suzaku* observations of the pulsar during the giant X-ray outburst.

2 OBSERVATIONS AND DATA ANALYSIS

The fifth Japanese X-ray satellite, *Suzaku*, was launched on 2005 July 10 (Mitsuda et al. 2007). The X-ray imaging spectrometers (XISs; Koyama et al. 2007) and the hard X-ray detectors (HXDs; Takahashi et al. 2007) onboard *Suzaku* covered the 0.5–600 keV range. The XISs are CCD cameras located at the focal points of each of the four X-ray telescopes (XRTs; Serlemitsos et al. 2007). XIS-0, XIS-2 and XIS-3 are front-illuminated while XIS-1 is back-illuminated. The hard X-ray unit of *Suzaku* consists of two non-imaging detectors, e.g. HXD/PIN and HXD/GSO. HXD/PIN consists of silicon diode detectors that work in the 10–70 keV range and HXD/GSO consists of crystal scintillator detectors covering the 40–600 keV range. The field of view of XIS is $17.8' \times 17.8'$ in open window mode. HXD/GSO has the same field of view of $34' \times 34'$ as HXD/PIN up to 100 keV.

Target of opportunity observations of KS 1947+300 were carried out with *Suzaku* at two epochs during its giant outburst in October-November 2013. The first observation was performed on 2013 October 22, close to the peak of the outburst for an effective exposure of ∼29 ks. The second observation was carried out on 2013 November 22–23 at the peak of the outburst for an effective exposure of ∼8 ks and 32 ks for XIS and HXD, respectively. The XIS detectors were operated in normal and burst clock mode with 2 s and 0.5 s time resolutions for the first and second observations, respectively. Both the observations were carried out in the 'XIS nominal' position. A *Swift/BAT* monitoring light curve of the pulsar in the 15–50 keV range covering the giant X-ray outburst is shown in Figure 1. The arrow marks in the figure represent the date of *Suzaku* observa-

Table 1 Pulse Period History of KS 1947+300 during its 2013 Giant Outburst

MJD	Date	Period (s)	Reference
56586.79	2013–10–21	18.80584(16)	Fürst et al. (2014)
56587.22	2013–10–22	18.8088(1)	present work
56618.61	2013–11–22	18.7878(1)	present work
56618.91	2013–11–22	18.78399(7)	Fürst et al. (2014)
56635.75	2013–12–09	18.77088(6)	Fürst et al. (2014)
57053	2015–01–31	18.76255	Finger et al. (2015)

tions of the pulsar. In the present study, we used the publicly available data with Observation IDs: 908001010 and 908001020 (hereafter Obs.1 and Obs.2 respectively).

2.1 Data Reduction

Unfiltered XIS and HXD event data were reprocessed by using the *aepipeline* task in the Heasoft (version 6.16) analysis package. Calibration database (CALDB) files released on 2012 November 06 (XIS) and 2011 September 13 (HXD) were used during data reprocessing. Cleaned event files generated after reprocessing were used in the present study. The *aebarycen* task of FTOOLS was applied on the cleaned event data to neutralize the effects of motions of the satellite and the Earth around the Sun. We checked the effect of thermal flexing by applying the attitude correction S-lang script *aeattcor.sl*[1] on data from the XISs. After attitude correction, the XIS cleaned events were examined for possible photon pile-up by using the S-lang script *pile_estimate.sl*[2]. During Obs.1, we detected a pile-up of $\sim$31%, 21% and 33% at the centers of XIS-0, XIS-1 and XIS-3 images, respectively. Therefore, an annulus region with inner and outer radii of 75″ and 200″ was chosen to reduce the pile-up below 4%. As in the case of Obs.1, we estimated photon pile-up for Obs.2 which was found to be $\sim$15%, 12% and 18% at the centers of XIS-0, XIS-1 and XIS-3 images, respectively. An annulus region with inner and outer radii of 35″ and 200″ was considered for the pile-up correction in the second observation. The light-curves and spectra of the pulsar were extracted from the XIS cleaned event data by applying the annulus regions in the *XSELECT* package. Background light curves and spectra were accumulated from a source free region in the XIS image frame. Response and effective area files for XISs were created from the "resp=yes" task during the spectral extraction in *XSELECT*. HXD/PIN and HXD/GSO source light curves and spectra were extracted from the cleaned event data by applying the GTI selection in *XSELECT*. The PIN and GSO background light curves and spectra were generated in a similar manner from the simulated tuned non-X-ray background event data provided by the instrument team. The response file released in June 2011 was used for HXD/PIN for both the observations. However, GSO response and additional effective area files released on 2010 May 24 and 2010 May 26, respectively, were used while analyzing HXD/GSO data.

[1] *http://space.mit.edu/ASC/software/suzaku/aeattcor.sl*

[2] *http://space.mit.edu/ASC/software/suzaku/pile_estimate.sl*

3 TIMING ANALYSIS

Source and background light curves were extracted from the reprocessed and barycentric corrected XISs, PIN and GSO event data with time resolutions of 2 s, 1 s, 1 s for Obs.1 and 0.5 s, 1 s, 1 s for Obs.2, respectively. The χ^2-maximization technique was applied to search for the periodicity in the background subtracted XIS and PIN light curves. Pulsations at periods of 18.8088(1) and 18.7878(1) s were detected in the light curves obtained from the first and second *Suzaku* observations, respectively. Though the observations were carried out within a time interval of one month, the decrease of the pulse period during a later epoch suggests that the pulsar was spinning up. The pulse period history of KS 1947+300, obtained from *NuSTAR* and *Suzaku* observations during the October-November 2013 outburst, is given in Table 1. Decreasing values of the spin period with time confirmed that the pulsar was spinning-up during the outburst. A recent measurement of pulse period of KS 1947+300 in the January-February 2015 outburst (see Table 1) also indicated the long term spin-up trend in the pulsar.

Pulse profiles of the pulsar in different energy bands that were generated from the XIS, PIN and GSO light curves, obtained from both observations, are shown in Figures 2 and 3. During the first observation, the soft X-ray pulse profile (below 5 keV) was found to be smooth and single peaked. However, with the increase in energy, a narrow dip-like feature appeared in the pulse profile and became prominent in the 30–40 keV range. Beyond this energy, the depth of the dip decreased and disappeared from the pulse profiles in the 70–100 keV range. During the second observation, the pulse profiles were found to show a similar type of energy dependence as seen during the first observation. X-ray pulsations in the light curves were detected up to $\sim$120 keV and $\sim$150 keV during the first and second observations, respectively. Absorption dips in the pulse profiles of BeXB pulsars during X-ray outbursts are found to be prominent in soft X-rays but weak in hard X-ray bands (Paul & Naik 2011 and references therein; Naik et al. 2013; Naik & Jaisawal 2015). However, in the case of *Suzaku* observations of KS 1947+300, the dip was found to be absent in the soft X-ray pulse profiles and prominent in the hard X-ray pulse profiles. It is, therefore, interesting to investigate the spectral properties of the pulsar to understand the causes of the absence/presence of an absorption dip in soft/hard X-ray pulse profiles.

4 SPECTRAL ANALYSIS

4.1 Pulse-Phase Averaged Spectroscopy

We performed phase-averaged spectroscopy of KS 1947+300 by using data from both *Suzaku* observations carried out during the giant outburst. Data from

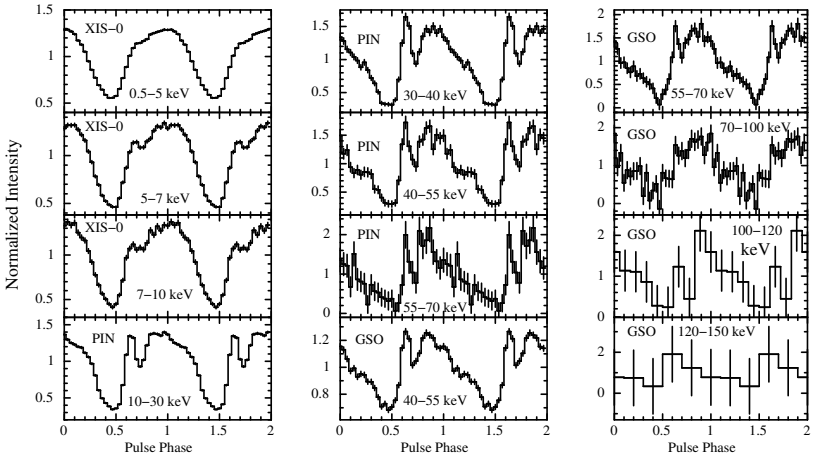

Fig. 2 Energy-resolved pulse profiles of KS 1947+300 obtained from XIS-0, HXD/PIN and HXD/GSO light curves at various energy ranges obtained from the first *Suzaku* observation of the pulsar on 2013 October 22. The error bars represent 1σ uncertainties. Two pulses in each panel are shown for clarity.

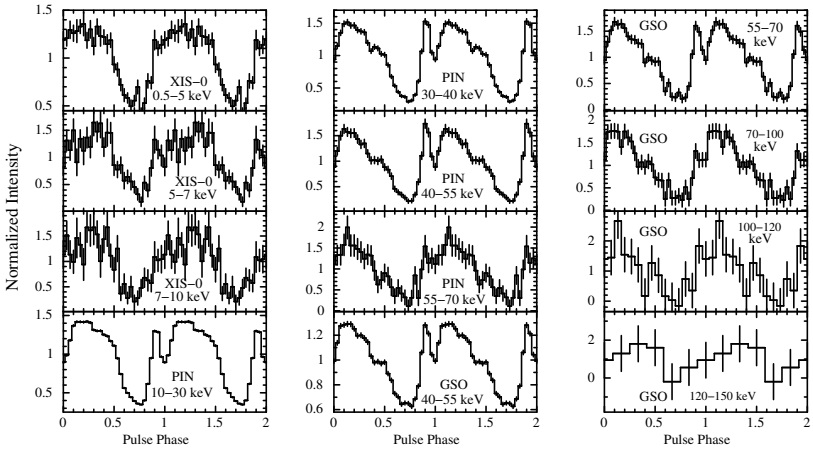

Fig. 3 Energy-resolved pulse profiles of KS 1947+300 obtained from XIS-0, HXD/PIN and HXD/GSO light curves at various energy ranges, during the second *Suzaku* observation. The presence of a dip-like feature can be clearly seen in the pulse profiles. The error bars represent 1σ uncertainties. Two pulses in each panel are shown for clarity.

XIS-0, XIS-1, XIS-3, PIN and GSO detectors were used in our analysis. The procedure followed to extract source and background spectra was described in the earlier section. To improve statistics, we re-binned the source spectra obtained from XISs and PIN event data to have a minimum of 20 counts per energy channel. However, GSO spectra were grouped as suggested by the instrument team. Like other bright X-ray sources where a systematic error of up to 3% was added to XIS spectra (Cyg X-1; Nowak et al. 2011), a systematic error of 1% was added to XIS spectra of KS 1947+300 for the cross calibration issues between back and front illuminated CCDs. Simultaneous spectral fitting was carried out in the $\sim$1–110 keV range for both observations by using the *XSPEC* (version 12.8.2) package. During spectral fitting, data in the ranges of 1.7–1.9 keV and 2.2–2.4 keV were ignored due to the presence of known Si and Au edges in XISs spectra. All the model parameters were tied together except the values of relative normalization of detectors which were kept free during simultaneous spectral fitting.

We used a high-energy cut-off power law, a cut-off power law and the Negative and Positive power law with EXponential cutoff (NPEX) model to describe the pulsar continuum. We found that all three models can explain the continuum spectrum well. Along with the interstellar absorption, a blackbody component for the soft X-ray excess and a Gaussian function for iron emission were required to fit the spectra. Though the broad-band spectral fitting yielded an emission line at $\sim$6.5 keV with a width of $\sim$0.2 keV, careful investigations of the residuals near the line energy confirmed the presence of two iron emission lines at 6.4 and 6.7 keV. Therefore, we added Gaussian functions at 6.4 and 6.7 keV in our broad-band spectral fitting. We identified these lines as emission from neutral and He-like iron atoms. It was found that the addition of a partial covering component to the above continuum models improved the spectral fitting further with significant improvement in the χ^2 values ($\Delta\chi^2 \geq 70$). This component has been used to investigate the cause of absorption dips at certain phases of the pulse profiles of BeXB

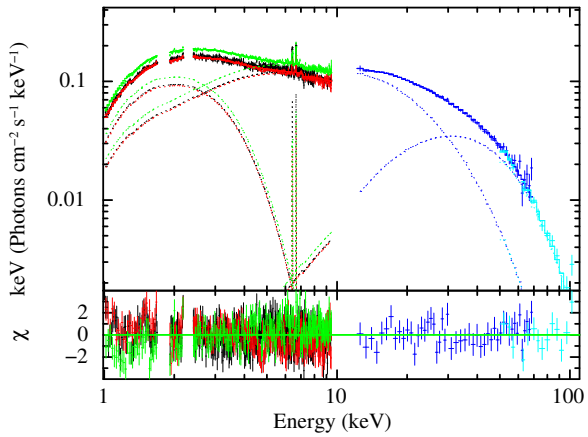

Fig. 4 Broad-band (1–110 keV energy range) spectrum of KS 1947+300 obtained with the XIS-0, XIS-1, XIS-3, PIN and GSO detectors of the first *Suzaku* observation during the October 2013 outburst along with the best-fit model comprising a partially absorbed NPEX continuum model, a blackbody component for soft X-ray excess, a Gaussian function for the iron emission line and fixed cyclotron absorption component. The contributions of the residuals to the χ^2 for each energy bin for the best-fit model are shown in the bottom panel.

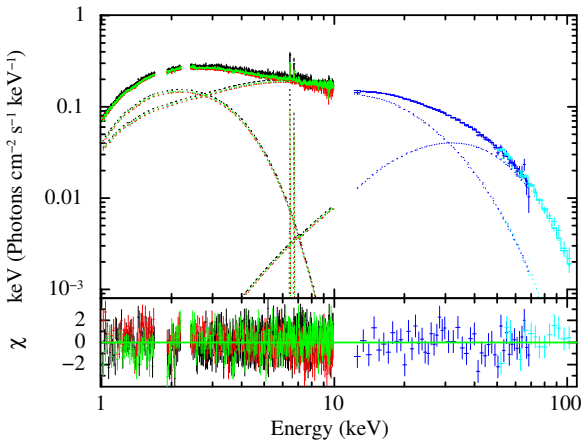

Fig. 5 1–110 keV energy spectrum of KS 1947+300 obtained with the XIS-0, XIS-1, XIS-3, PIN and GSO detectors of the second *Suzaku* observation during the October 2013 outburst along with the best-fit model comprised of a partially absorbed NPEX continuum model, a blackbody component for soft X-ray excess, a Gaussian function for the iron emission line and fixed cyclotron absorption component. The contributions of the residuals to the χ^2 for each energy bin for the best-fit model are shown in the bottom panel.

pulsars (Paul & Naik 2011). This component, therefore, was used to probe the cause of the observed absorption dip in the pulse profiles of KS 1947+300. A cyclotron line at 12.2 keV that was detected from *NuSTAR* observations was also included in the spectral model. Since *Suzaku* data cannot constrain the line region well, in our analysis, we fixed the cyclotron line parameters, i.e. line energy at 12.2 keV, width at 2.5 keV and depth at 0.16 as obtained from *NuSTAR* observations (Fürst et al. 2014). Among the three continuum models, the partial covering NPEX model along with other spectral components was found to be the best-fit model for both *Suzaku* observations.

Best-fitted spectral parameters obtained from all three models are given in Table 2 for both observations. The energy spectra for the partial covering NPEX continuum model along with residuals are shown in Figure 4 and 5 for the first and second *Suzaku* observations, respectively. The values of additional absorption column density ($N_{\rm H_2}$) were found to be significantly higher than the values of Galactic absorption column density ($N_{\rm H_1}$) (Table 2). The pulsar spectrum was marginally hard at the peak of the outburst, i.e. during the second observation compared to the first observation. The soft excess component was found to be stronger during the second observation (peak of the outburst) with higher values of blackbody temperature and flux compared to those during the first observation.

4.2 Pulse-Phase Resolved Spectroscopy

To investigate the nature of the absorption dip in hard X-ray pulse profiles, as well as the nature of the soft excess component and the evolution of other spectral parameters during both *Suzaku* observations, pulse-phase resolved spectroscopy was carried out by accumulating source spectra from XISs, PIN and GSO detectors in 9 and 10 phase bins for the first and second observations, respectively. Background spectra, response matrices and effective area files used in phase-averaged spectroscopy were also used in the phase-resolved spectroscopy. Simultaneous spectral fitting was carried out for phase-resolved spectra obtained from both observations by using a partial covering NPEX continuum model along with other components. During fitting, the equivalent Galactic hydrogen column density ($N_{\rm H_1}$; expected to be constant along the source direction), energy and width of iron emission lines, cyclotron line parameters (line energy, width and depth) and relative instrument normalizations were fixed at corresponding phase-averaged values. Due to a lack of sufficient photons, the iron emission lines were not resolved during the phase-resolved spectral fitting. It was found that the change in spectral parameters over the pulse phase are similar for both the observations and are shown in Figures 6 and 7 for the first and second observations, respectively. Pulse profiles of the pulsar obtained from XIS-0 and PIN light curves of both observations are shown in the top two panels of the left and right panels of Figures 6 and 7. Changes in the spectral parameters such as additional column density ($N_{\rm H_2}$), covering fraction, blackbody temperature for soft X-ray excess and soft X-ray excess flux with pulse phases are shown in subsequent panels on the left sides of Figures 6 and 7. The panels in the right side of Figures 6 and 7 show the changes in soft (1–10 keV) and hard X-ray (10–100 keV) fluxes, power-law photon index and cutoff energy.

All the spectral parameters plotted in Figures 6 and 7 were found to be variable with pulse phase of the pulsar. Additional column density was found to be marginally higher at the phase of the absorption dip in the hard X-

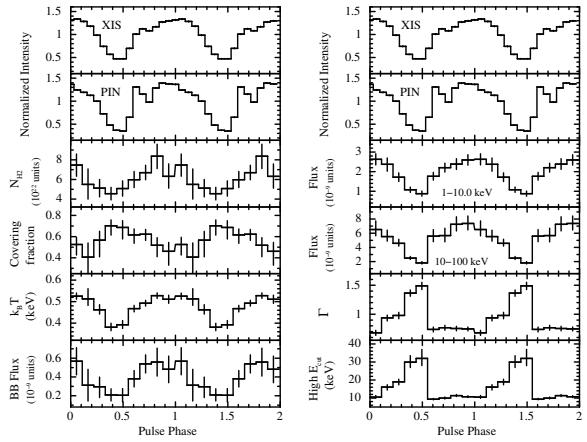

Fig. 6 Spectral parameters obtained from the phase-resolved spectroscopy of KS 1947+300 during the first *Suzaku* observation in October 2013. The first and second panels on both sides show pulse profiles of the pulsar in the 0.5–10 keV (XIS-0) and 10–70 keV (HXD/PIN) energy ranges. The values of $N_{\rm H_2}$, covering fraction, blackbody temperature and blackbody flux are shown in the third, fourth, fifth and sixth panels in the left side of the figure, respectively. The soft X-ray flux in the 1–10 keV range, hard X-ray flux in the 10–100 keV range, photon index and high energy cutoff are shown in the third, fourth, fifth and sixth panels in the right side of the figure, respectively. The blackbody flux and source fluxes in 1–10 and 10–100 keV are quoted in the units of 10^{-9} erg cm^{-2} s^{-1}. The errors in the figure are estimated at the 90% confidence level.

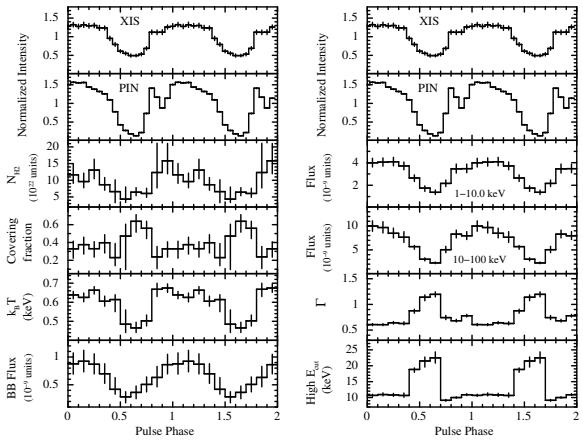

Fig. 7 Spectral parameters obtained from the phase-resolved spectroscopy of KS 1947+300 during the second *Suzaku* observation in November 2013. The first and second panels in both sides show pulse profiles of the pulsar in the 0.5–10 keV (XIS-0) and 10–70 keV (HXD/PIN) energy ranges. The values of $N_{\rm H_2}$, covering fraction, blackbody temperature and blackbody flux are shown in the third, fourth, fifth and sixth panels in the left side of the figure, respectively. The soft X-ray flux in the 1–10 keV range, hard X-ray flux in the 10–100 keV range, photon index and high energy cutoff are shown in the third, fourth, fifth and sixth panels in the right side of the figure, respectively. The blackbody flux and source fluxes in 1–10 and 10–100 keV are expressed in units of 10^{-9} erg cm^{-2} s^{-1}. The errors in the figure are estimated at the 90% confidence level.

ray pulse profile. Blackbody temperature, blackbody flux and source flux in the 1–10 keV range showed a similar variation pattern as the soft X-ray pulse profile over pulse phases. This confirmed the pulsating nature of the soft X-ray excess component in phase with the source flux. The values of power-law photon index and high energy cutoff were found to be higher during the main dip phases. The dependence of several spectral parameters on additional column density and source flux in the 1–10 keV range were investigated and are shown in Figures 8 and 9. The left panels show the dependence of power-law photon index and blackbody temperature on the additional column density whereas the right panels show the dependence of blackbody temperature and blackbody flux on the source flux in the 1–10 keV range. It was found that the blackbody temperature and flux showed a positive correlation with the soft X-ray flux in the 1–10 kev range. The value of power-law photon index was found to be high at a low value of additional column density ($N_{\rm H_2}$) and decreased with the increase in $N_{\rm H_2}$.

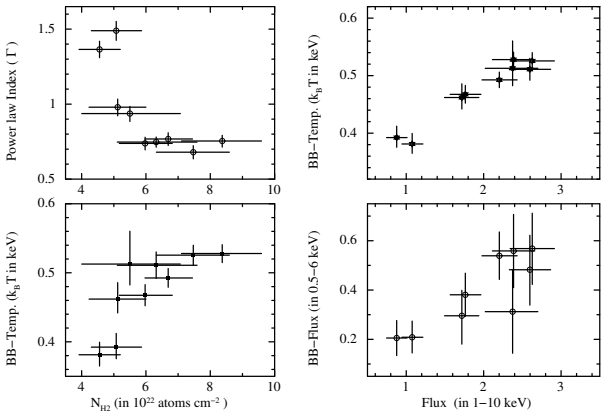

Fig. 8 Dependence of different spectral parameters obtained from the phase-resolved spectroscopy of KS 1947+300 during the first *Suzaku* observation. The blackbody flux and 1–10 keV source flux are quoted in the units of 10^{-9} erg cm^{-2} s^{-1}.

5 DISCUSSION AND CONCLUSIONS

5.1 Spin-Period and Magnetic Field of the Pulsar

KS 1947+300 was observed with *Suzaku* at two epochs during its 2013 X-ray outburst. Although the observations were only a month apart, estimated spin periods of the pulsar during both the observations were found to be different. The spin period during the second observation was smaller than the first observation, indicating the pulsar was spinning up during the X-ray outburst. While comparing the recent measurements of the spin period of the pulsar with what was reported from observations with several other observatories (as quoted in Table 1), it was found that the pulsar was continuously spinning up during the entire 2013 X-ray outburst. During X-ray outbursts, spinning-up of the neutron star is expected due to transfer of angular momentum from accreting matter at the magnetic poles. Ghosh & Lamb (1979) formulated the dependence of the spin-up rate of a pulsar on its luminosity as $\dot{P} \propto L^{6/7}$.

Table 2 Best-fitting spectral parameters (with 90% errors) obtained from two *Suzaku* observations of KS 1947+300 during the 2013 outburst. Model-1: partial covering NPEX model with Gaussian components and a cyclotron absorption line; Model-2: partial covering high-energy cutoff model with Gaussian components and a cyclotron absorption line; Model-3: partial covering cutoff power law model with Gaussian components and a cyclotron absorption line. The cyclotron line parameters were fixed at the values from Fürst et al. (2014).

Parameter	October 2013 (Obs.1)			November 2013 (Obs.2)		
	Model-1	Model-2	Model-3	Model-1	Model-2	Model-3
$N_{\rm H_1}{}^a$	0.50±0.02	0.50±0.02	0.52±0.02	0.48±0.02	0.50±0.02	0.53±0.02
$N_{\rm H_2}{}^b$	7.6±1.0	8.2±1.1	7.6±1.1	11.3±2.5	10.7±1.7	12.1±4.8
Covering fraction	0.44±0.06	0.45±0.06	0.43±0.06	0.35±0.06	0.35±0.06	0.27±0.07
Photon Index (Γ)	0.67±0.03	0.95±0.04	0.92±0.05	0.62±0.04	0.93±0.04	0.93±0.03
$E_{\rm cut}$ (keV)	10.2±0.3	5.4±0.4	20.2±0.9	10.6±0.4	5.9±0.3	21.6±0.7
$E_{\rm fold}$ (keV)	–	21.0±0.7	–	–	21.6±0.7	–
Blackbody temp. kT (keV)	0.54±0.02	0.56±0.02	0.54±0.02	0.63±0.03	0.65±0.02	0.65±0.03
Blackbody flux^c	0.88±0.13	0.96±0.13	0.77±0.13	1.34±0.19	1.40±0.20	1.02±0.19
Emission lines						
Fe $K\alpha$ line energy (keV)	6.42±0.03	6.42±0.03	6.42±0.03	6.45±0.02	6.45±0.02	6.45±0.02
Width of Fe line (keV)	$0.01^{+0.06}_{-0.01}$	$0.01^{+0.06}_{-0.01}$	$0.01^{+0.06}_{-0.01}$	$0.01^{+0.04}_{-0.01}$	$0.01^{+0.04}_{-0.01}$	$0.01^{+0.04}_{-0.01}$
Eq. width of Fe line (eV)	18±2	19±2	19±2	20±3	20±3	22±2
Line energy (keV)	6.66±0.05	6.66±0.05	6.66±0.05	6.71±0.04	6.71±0.04	6.71±0.02
Line width (keV)	$0.01^{+0.07}_{-0.01}$	$0.01^{+0.07}_{-0.01}$	$0.01^{+0.07}_{-0.01}$	$0.01^{+0.07}_{-0.01}$	$0.01^{+0.07}_{-0.01}$	$0.01^{+0.07}_{-0.01}$
Equivalent width (eV)	17±2	18±2	18±2	11±3	11±3	13±3
Source flux						
Flux^c (1–10 keV)	2.6±0.2	2.7±0.2	2.6±0.2	4.3±0.4	4.3±0.4	4.1±0.4
Flux^c (10–70 keV)	5.4±0.5	5.3±0.4	5.3±0.3	6.6±0.6	6.5±0.5	6.5±0.4
Flux^c (70–100 keV)	0.21±0.03	0.27±0.02	0.27±0.02	0.38±0.03	0.38±0.03	0.38±0.02
Reduced χ^2	1.18 (942)	1.25 (970)	1.25 (971)	1.08 (970)	1.10 (942)	1.13 (971)

Notes: ^{a}: Equivalent hydrogen column density (in 10^{22} atom cm^{-2} units); ^{b}: Additional hydrogen column density (in 10^{22} atom cm^{-2} units); ^{c}: Absorption corrected flux in units of 10^{-9} erg cm^{-2} s^{-1}.

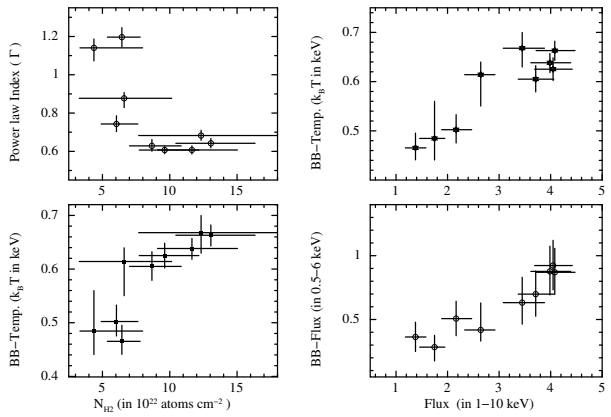

Fig. 9 Dependence of different spectral parameters obtained from the phase-resolved spectroscopy of KS 1947+300 during the second *Suzaku* observation. The blackbody flux and 1–10 keV source flux are quoted in units of 10^{-9} erg cm^{-2} s^{-1}.

In the present work, the pulsar spin period was found to be 18.7878 s (*Suzaku*) at the peak of the outburst which decreased to 18.77088 s (*NuSTAR* observation) during the decay of the outburst (see Table 1). The observed spin-up of KS 1947+300 can be attributed to the change in angular momentum due to the torque exerted by accreting matter on the neutron star. A similar type of rapid spin-up was also observed during the declining phase of the 2001 outburst of the pulsar (Naik et al. 2006).

The pulsar was showing a spin-up trend during *Suzaku* and *NuSTAR* observations. The observed spin-up (angular frequency) rate ($\dot{\omega}_{\rm su}$) can be used to estimate the magnetic field of the pulsar by considering the quasi-spherical settling accretion theory (Shakura et al. 2012; Postnov et al. 2015). According to this theory,

$$\dot{\omega}_{\rm su} \simeq 10^{-9}[{\rm Hz\ d^{-1}}]\ \Pi_{\rm su}\ \mu_{30}^{1/11} v_8^{-4} \left(\frac{P_b}{10\ d}\right)^{-1} \dot{M}_{16}^{7/11}, \quad (1)$$

where $\dot{\omega}_{\rm su}$ is spin-up rate which is estimated to be 1.27×10^{-5}[Hz d^{-1}] (present case) and $\Pi_{\rm su}$ is the dimensionless parameter from settling accretion theory. The value of $\Pi_{\rm su}$ is independent of the system and is in the range of $\sim$4.6 to 10 (Shakura et al. 2012; Postnov et al. 2015). In the present case, $\Pi_{\rm su}$ was assumed to be 4.6. The dipole magnetic moment of the neutron star μ_{30}=$\mu/10^{30}$[G cm^3] and is related to the magnetic field (B)

through the relation $\mu = BR^3/2$ (R is the neutron star radius, assumed to be 10 km). Stellar wind velocity $v_8 = v/10^8$ [cm s^{-1}] is considered to be 200 km s^{-1} for typical BeXBs (Waters et al. 1988). The mass accretion rate $\dot{M}_{16}$=$\dot{M}/10^{16}$[g s^{-1}] for the luminosity of 10^{38} erg s^{-1} was estimated to be $\dot{M}_{16} = 100$ during *Suzaku* observations. The orbital period $P_{\rm b}$ of KS 1947+300 is 40.42 d (Galloway et al. 2004). Using the above parameters, the magnetic field of the pulsar was estimated to be $\sim$1.2$\times10^{12}$ G. The estimated value of the magnetic field by using the observed spin-up rate in KS 1947+300 was found to agree with that obtained from the detection of the cyclotron absorption line at 12.2 keV.

5.2 Pulse Profiles

In the present work, the pulse profile of KS 1947+300 was found to be simple at lower energies. As the energy increases, a dip like structure appears in the pulse profile and is detected up to 70 keV. The depth of the dip is found to increase with energy and is maximum in the 30–40 keV range. Such type of behavior is not generally seen in pulse profiles of other BeXB pulsars. We tried to investigate the cause of the absorption dip in pulse profiles at hard X-rays ($>$10 keV) through phase-resolved spectroscopy. A marginal enhancement in the additional column density at the dip phase was detected. Such a low value ($\leq$20$\times10^{22}$ cm^{-2}) of additional column density, however, cannot absorb the hard X-ray photons up to $\sim$70 keV. KS 1947+300 was also observed at different luminosity levels with several observatories such as *BeppoSAX*, *RXTE*, *INTEGRAL* and *NuSTAR*. The pulse profiles obtained from these observations were found to be similar to that obtained from *Suzaku* observations. The dip was only seen in hard X-rays (Galloway et al. 2004; Tsygankov & Lutovinov 2005; Naik et al. 2006; Fürst et al. 2014). Therefore, the presence of the dip in hard X-ray pulse profiles of KS 1947+300 is possibly intrinsic to the pulsar.

In general, the pulse profiles of BeXB pulsars are seen to be strongly energy and luminosity dependent. Single or multiple absorption dips, prominent at soft X-ray, are seen in the pulse profiles of these pulsars (Paul and Naik 2011 and references therein). With an increase in energy, the depth of the dip decreases and becomes invisible at higher energies. It is widely believed that these dips in the pulse profile are due to obscuration/absorption of soft X-ray photons by matter present close to the neutron star. In some cases, single or multiple dips were observed at high energies, e.g. up to 70 keV in pulse profiles of EXO 2030+275 (Naik et al. 2013; Naik & Jaisawal 2015). The presence of additional dense matter at dip phases was detected from phase-resolved spectroscopy and was interpreted as the cause of absorption dips in the pulse profiles of EXO 2030+375. In KS 1947+300 (present work), however, the origin of the dip in hard X-ray pulse profiles (up to $\sim$70 keV) is not due to the presence of additional matter at a certain phase of the pulsar.

The pulse profile of the pulsars can be affected by cyclotron resonance scattering and geometrical effects. These effects can play a vital role and shape the anomaly or dip in the pulse profiles. In KS 1947+300, a cyclotron absorption line was detected at $\sim$12.2 keV (Fürst et al. 2014). The beam function of an accreting pulsar can be affected by the presence of strong cyclotron resonance scattering which can produce a significant change in the pulse profile, e.g. phase-shift (lag) (Schönherr et al. 2014). Similar effects were detected in BeXB pulsars such as V 0332+53 (Tsygankov et al. 2006), 4U 0115+63 (Ferrigno et al. 2011) and GX 304–1 (Jaisawal et al. 2016). However, this is not the case in KS 1947+300 as the strength of the observed dip increased with energy and became prominent in the $\sim$30–40 keV energy range. Around this energy, however, the influence of cyclotron resonance scattering is not as effective as compared to energies closer to $\sim$12 keV. In addition, any significant change in the pulse profiles (beam pattern) or phase-lags was not observed in the energy resolved pulse profiles (Figs. 2 and 3). Therefore, we expect that the cyclotron scattering is not causing the hard X-ray dip in the pulse profiles of KS 1947+300. Alternatively, the presence of a single dip in hard X-ray profiles suggests the direct viewing of the pole of the neutron star through the accretion column. At such high luminosity ($\sim10^{38}$ erg s^{-1}) like the one found by the *Suzaku* observations of KS 1947+300, a radiation pressure dominated shock is expected to form above the surface of the neutron star which can absorb the photons up to higher energies.

In this case, the position of the absorption dip should be at the peak of the pulse profiles. However, the asymmetric phase position of the dip with respect to the main dip in pulse profiles (Figs. 2 and 3) discards the hypothesis of direct viewing of the pulsar along the magnetic axis. It is accepted that the pulse profile of X-ray pulsars depends on the geometry and viewing angle of the emission region or accretion column (Kraus et al. 1995; Caballero et al. 2011; Sasaki et al. 2012). We suggest that the dip in the hard X-ray pulse profiles of KS 1947+300 is due to these geometrical effects. The dip was absent in the soft X-ray pulse profiles. The presence of strong soft X-ray excess (which was found pulsating in phase with the neutron star) may cancel the effect of the absorption dip, producing single pulse profiles in soft X-ray bands.

5.3 Spectroscopy

In this paper, broad-band phase-averaged and phase-resolved spectra of KS 1947+300 are presented by using two *Suzaku* observations of the 2013 giant outburst. During both observations, the values of estimated Galactic column density were comparable. However, the values of the additional column density were found to be significantly higher than the Galactic value. The higher values of additional absorption column density indicate the presence

of additional matter near the neutron star during the X-ray outburst. During both the observations, a soft X-ray excess was clearly detected and its temperature was found to be high at the peak of the outburst (second observation). Assuming the blackbody emitting region to be spherically symmetric, the radius of the soft X-ray excess emitting region in KS 1947+300 is estimated to be ∼29–31 km. It implies that the soft X-ray excess emitting region is close to the neutron star surface. The pulsating nature of the soft X-ray excess in KS 1947+300 agrees with the above argument. Therefore, the accretion column and/or accretion streams are the most probable origin site of soft X-ray excess emission in KS 1947+300 (Naik & Paul 2002; Naik & Paul 2004; Hickox et al. 2004).

Apart from the detection of soft X-ray excess and the presence of additional matter around the pulsar, a change in the power-law photon index and high energy cutoff with pulse phase was seen in KS 1947+300. A similar type of variation was also seen in other BeXB pulsars such as EXO 2030+275 (Naik et al. 2013; Naik & Jaisawal 2015). Narrow iron Kα and He-like iron emission lines at ∼6.4 and 6.7 keV were detected during both the observations. During *BeppoSAX* observations of KS 1947+300 in the 2001 outburst, an emission line at 6.7 keV was detected whereas the iron Kα line was absent in the pulsar spectra (Naik et al. 2006). The 6.7 keV line was identified as the emission feature from helium-like iron atoms. A cyclotron absorption feature at ∼12.2 keV was detected in KS 1947+300 from *NuSTAR* observations during the 2013 outburst (Fürst et al. 2014). Detection of the cyclotron line is a unique tool to directly estimate the magnetic field of the pulsar by using the 12-B-12 rule or $E_{\rm cyc} = 11.6 B_{12} \times (1+z)^{-1}$. Using the detected cyclotron absorption line at 12.2 keV, the strength of the surface magnetic field was estimated to be $\sim 1.1 \times 10^{12} (1+z)$ G (Fürst et al. 2014). Though the pulsar was observed with *NuSTAR* at three epochs, the cyclotron line was only detected during the second observation and there was no signature of the presence of its harmonics in the pulsar spectrum. We also did not find harmonics of the 12.2 keV cyclotron line in pulsar spectra obtained from *Suzaku* observations. There are several pulsars where a fundamental cyclotron line is seen in the broad-band spectra without the detection of its harmonics, e.g. Cen X-3 (Suchy et al. 2008; Naik et al. 2011), Swift J1626.6–5156 (DeCesar et al. 2013), and IGR J17544-2619 (Bhalerao et al. 2015). The 1–100 keV luminosity of the pulsar was estimated to be $\sim 9.8 \times 10^{37}$ and 1.3×10^{38} erg s^{-1} during the first and second *Suzaku* observations, respectively. Critical luminosity was calculated to investigate the luminosity regime of the pulsar by assuming parameters of a canonical neutron star with cyclotron line energy at 12.2 keV in the relation of Becker et al. (2012). This was estimated to be $\sim 1.6 \times 10^{37}$ erg s^{-1}. It is clear that the pulsar was accreting in the super-Eddington regime (above the critical luminosity) during the October 2013 (present work) and November 2000 (Naik et al. 2006) outbursts.

In summary, we reported on the timing and broad-band spectral properties of the pulsar KS 1947+300 by using *Suzaku* observations taken during the 2013 outburst. Soft X-ray pulse profiles were found to be smooth and single peaked. However, hard X-ray pulse profiles showed the presence of an absorption dip like feature. The 1–110 keV broad-band spectrum of the pulsar was described with a partially absorbed NPEX continuum model along with a blackbody component. Phase-resolved spectroscopy revealed marginal enhancement in the additional column density at the dip phase, which suggests that the dip is not because of the absorption of hard X-ray photons. Another mechanism such as a geometrical effect could be a possible cause for the presence of a dip in the hard X-ray pulse profiles of KS 1947+300. Detection of pulsation in the soft X-ray excess flux confirmed that the emitting region is close to the neutron star, e.g. near the accretion column. The presence of soft X-ray excess may be the cause of the absence of the dip in soft X-ray profiles. We estimated the magnetic field of the pulsar by using the observed spin-up rate during *Suzaku* and *NuSTAR* observations. The value was found to be 1.2×10^{12} G and comparable to that obtained from the cyclotron line energy.

Acknowledgements We sincerely thank the referee for his valuable comments and suggestions which improved the paper significantly. The research work at the Physical Research Laboratory is funded by the Department of Space, Government of India. The authors would like to thank all the members of the *Suzaku* mission for their contributions in the instrument preparation, spacecraft operation, software development and in-orbit instrumental calibration. This research has made use of data obtained through HEASARC Online Service, provided by NASA/GSFC, in support of NASA High Energy Astrophysics Programs.

References

Becker, P. A., Klochkov, D., Schönherr, G., et al. 2012, A&A, 544, A123

Bhalerao, V., Romano, P., Tomsick, J., et al. 2015, MNRAS, 447, 2274

Borozdin, K., Gilfanov, M., Sunyaev, R., et al. 1990, Soviet Astronomy Letters, 16, 345

Caballero, I., Kraus, U., Santangelo, A., Sasaki, M., & Kretschmar, P. 2011, A&A, 526, A131

Caballero, I., & Wilms, J. 2012, Mem. Soc. Astron. Italiana, 83, 230

Chakrabarty, D., Koh, T., Bildsten, L., et al. 1995, ApJ, 446, 826

DeCesar, M. E., Boyd, P. T., Pottschmidt, K., et al. 2013, ApJ, 762, 61

Ferrigno, C., Falanga, M., Bozzo, E., et al. 2011, A&A, 532, A76

Finger, M. H., Jenke, P. A., & Wilson-Hodge, C. A. 2015, The Astronomer's Telegram, 7017

Fürst, F., Pottschmidt, K., Wilms, J., et al. 2014, ApJ, 784, L40
Galloway, D. K., Morgan, E. H., & Levine, A. M. 2004, ApJ, 613, 1164
Ghosh, P., & Lamb, F. K. 1979, ApJ, 234, 296
Hickox, R. C., Narayan, R., & Kallman, T. R. 2004, ApJ, 614, 881
Jaisawal, G. K., Naik, S., & Epili, P. 2016, MNRAS, 457, 2749
James, M., Paul, B., Devasia, J., & Indulekha, K. 2010, MNRAS, 407, 285
Koyama, K., Tsunemi, H., Dotani, T., et al. 2007, PASJ, 59, 23
Kraus, U., Nollert, H.-P., Ruder, H., & Riffert, H. 1995, ApJ, 450, 763
Levine, A., & Corbet, R. 2000, IAU Circ., 7523
Mitsuda, K., Bautz, M., Inoue, H., et al. 2007, PASJ, 59, 1
Naik, S., & Paul, B. 2002, Journal of Astrophysics and Astronomy, 23, 27
Naik, S., & Paul, B. 2004, ApJ, 600, 351
Naik, S., Callanan, P. J., Paul, B., & Dotani, T. 2006, ApJ, 647, 1293
Naik, S., Paul, B., & Ali, Z. 2011, ApJ, 737, 79
Naik, S., Maitra, C., Jaisawal, G. K., & Paul, B. 2013, ApJ, 764, 158
Naik, S., & Jaisawal, G. K. 2015, RAA (Research in Astronomy and Astrophysics), 15, 537
Negueruela, I., Israel, G. L., Marco, A., Norton, A. J., & Speziali, R. 2003, A&A, 397, 739
Nowak, M. A., Hanke, M., Trowbridge, S. N., et al. 2011, ApJ, 728, 13
Okazaki, A. T., & Negueruela, I. 2001, A&A, 377, 161
Paul, B., & Naik, S. 2011, Bulletin of the Astronomical Society of India, 39, 429
Postnov, K. A., Mironov, A. I., Lutovinov, A. A., et al. 2015, MNRAS, 446, 1013
Reig, P. 2011, Ap&SS, 332, 1
Sasaki, M., Müller, D., Kraus, U., Ferrigno, C., & Santangelo, A. 2012, A&A, 540, A35
Schönherr, G., Schwarm, F.-W., Falkner, S., et al. 2014, A&A, 564, L8
Serlemitsos, P. J., Soong, Y., Chan, K.-W., et al. 2007, PASJ, 59, 9
Shakura, N., Postnov, K., Kochetkova, A., & Hjalmarsdotter, L. 2012, MNRAS, 420, 216
Skinner, G. K. 1989, IAU Circ., 4850
Suchy, S., Pottschmidt, K., Wilms, J., et al. 2008, ApJ, 675, 1487
Swank, J., & Morgan, E. 2000, IAU Circ., 7531
Takahashi, T., Abe, K., Endo, M., et al. 2007, PASJ, 59, 35
Tsygankov, S. S., & Lutovinov, A. A. 2005, Astronomy Letters, 31, 88
Tsygankov, S. S., Lutovinov, A. A., Churazov, E. M., & Sunyaev, R. A. 2006, MNRAS, 371, 19
Waters, L. B. F. M., van den Heuvel, E. P. J., Taylor, A. R., Habets, G. M. H. J., & Persi, P. 1988, A&A, 198, 200